ACS APPLIED MATERIALS & INTERFACES

www.acsami.org

Forum Article

Ortho-Substituted α-Phenyl Mannoside Derivatives Promoted Early-Stage Adhesion and Biofilm Formation of *E. coli* 83972

Zhiling Zhu, Yanxin Chen, Siheng Li, Hong Lin, Guoting Qin,* and Chengzhi Cai*

Cite This: *ACS Appl. Mater. Interfaces* 2020, 12, 21300–21310

Read Online

ACCESS | Metrics & More | Article Recommendations | Supporting Information

ABSTRACT: Prevention of catheter-associated urinary tract infection (CAUTI) over long-term usage of urinary catheters remains a great challenge. Bacterial interference using non-pathogenic bacteria, such as *E. coli* 83972, have been investigated in many pilot-scale clinical studies as a potentially nonantibiotic based strategy for CAUTI prevention. We have demonstrated that preforming a dense and stable biofilm of the nonpathogenic *E. coli* greatly enhances their capability to prevent pathogen colonization. Such nonpathogenic biofilms were formed by *E. coli* 83972 expressing type 1 fimbriae (*fim+ E. coli 83972*) on mannoside-presenting surfaces. In this work, we report the synthesis of a series of mannoside derivatives with a wide range of binding affinities, all being equipped with a handle for covalent attachment to silicone surfaces. We established a high-throughput competitive assay based on mannoside-modified particles and flow-cytometry to directly measure the binding affinity between the mannoside ligands and *fim + E. coli* 83972. We demonstrated that the bacterial adhesion and biofilm formation were strongly correlated to the binding affinity of the immobilized mannoside ligands. Mass spectrometry based proteomic analysis indicated a substantial difference in the proteome of the extracellular polymeric substance (EPS) secreted by biofilms on different mannoside surfaces, which might be related to the biofilm stability.

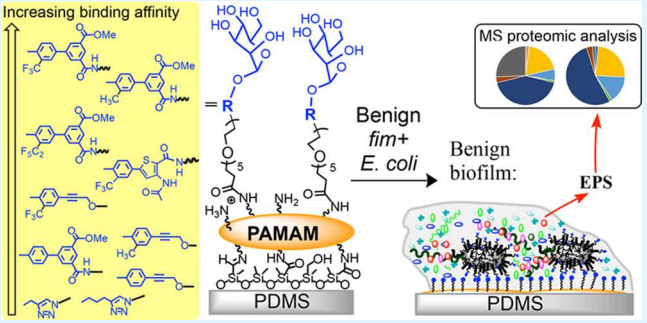

KEYWORDS: *mannoside, benign bacteria, FimH, biofilm, flow cytometry, CAUTI*

1. INTRODUCTION

A urinary tract infection (UTI) is a common healthcare-associated infection, accounting for more than 560,000 incidences and 13,000 deaths every year in the United States, as reported by the Centers for Disease Control and Prevention.[1] Up to 50% of women and 5% of men will experience a minimum of one UTI in their life.[2] The estimated annual UTI-associated costs for the healthcare industry were above $1.6 billion.[2] Most healthcare-associated UTI cases are caused by the use of urinary catheters, commonly known as catheter-associated urinary tract infection (CAUTI).[1]

A myriad of antimicrobial and antifouling strategies for urinary catheters have been developed and practiced clinically to prevent CAUTI.[3,4] However, they could not prevent pathogen colonization and biofilm formation in a eutrophic environment over long-term use.[5] In fact, uropathogens proliferate rapidly and generate plenty of biomass to envelope the bacterial colonies on the catheter surfaces, shielding against the antimicrobial agents and promoting development of resistance.[6] It is increasingly urgent to develop alternative, non-antibiotic-based strategies for long-term prevention of CAUTI, which are capable of persistent inhibition of pathogenic colonization on the catheter surfaces. Bacterial interference is potentially such a strategy being investigated using benign microorganisms, e.g. *Escherichia coli* 83972 and selected *Lactobacillus* species, to persistently outcompete uropathogens.[7,8] Our previous work showed that surfaces presenting D-mannoside derivatives were able to promote the adhesion by a strain of *E. coli* 83972 expressing type 1 fimabrae (*fim+ E. coli* 83972).[9] Using four mannoside derivatives with a relatively low binding affinity to FimH as measured in this work, our previous study suggested that the mannoside-FimH binding affinity was a key factor in controlling the initial *E. coli* 83972 adhesion and the resulting biofilm density and stability.[10,11] To confirm this and to evaluate the role of mannosides with much higher binding affinities to *fim+ E. coli* 83972 on biofilm formation, in this work, we synthesized a wide range of mannoside derivatives, including those reported to be among the most potent ligands to FimH. All are equipped with a handle for attachment onto silicone surfaces using our established method.[9]

Special Issue: Advances in Biocidal Materials and Interfaces

Received: October 2, 2019
Accepted: January 31, 2020
Published: February 28, 2020

https://dx.doi.org/10.1021/acsami.9b17868
ACS Appl. Mater. Interfaces 2020, 12, 21300–21310

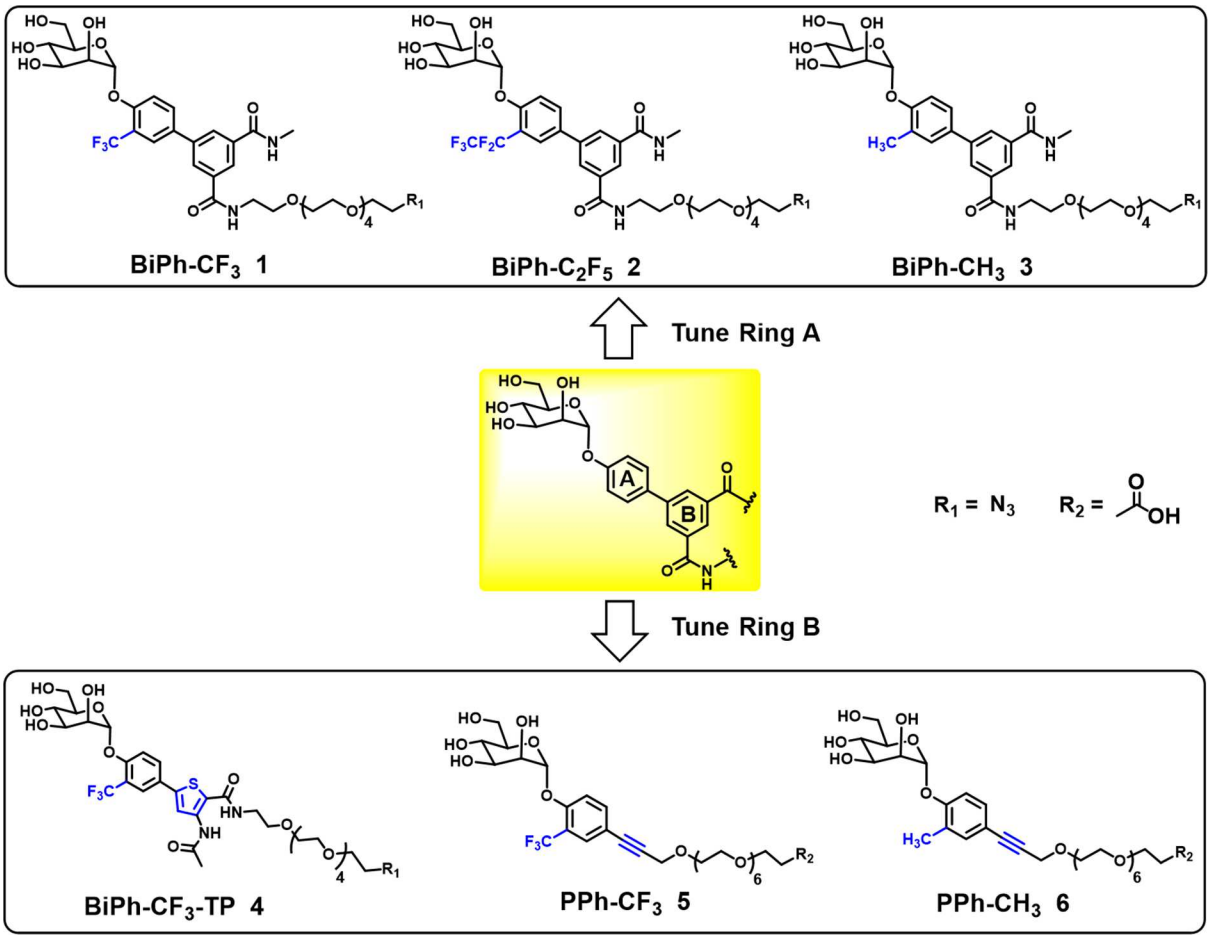

Figure 1. Illustration of structure tuning of mannoside ligands. The ortho-substituted α-phenyl mannosides are listed in the black boxes as **BiPh−CF_3** (**1**), **BiPh−C_2F_5** (**2**), **BiPh−CH_3** (**3**), **BiPh−CF_3-TP** (**4**), **PPh−CF_3** (**5**), and **PPh−CH_3** (**6**).

Type 1 fimbriae encoded by the functional fim operon is a principal adhesin during the initial adhesion of *E. coli* 83972. In particular, the FimH subunit locating at the tip of the fimbria comprises a mannoside-specific recognition domain (the lectin domain) and the pilin domain connecting to the pilus.[12−14] The X-ray crystallographic structure of FimH-mannoside complex showed that the mannosidic moiety is locked in the binding pocket by an extended hydrogen bonding network, where the glycosidic hydrophobic moiety interacts with two tyrosine residues (Tyr48 and Tyr137) at the entrance of the FimH binding domain,[15,16] namely, "tyrosine gate". Reports have shown that α-phenyl mannosides exhibited enhanced affinity with the FimH adhesin because the substitution of aglycones with aryl and alkyl chains resulted in enhancement of the hydrophobic stacking interactions with the FimH ridge.[17−19] Optimization of the ortho- and para-aryl substituents of the α-phenyl mannoside further increased the FimH binding affinity.[17,20] Recently, Sauer et al. systematically characterized the interactions between the FimH adhesin and the natural high-mannose type *N*-glycan binding epitopes.[21] Their results suggested that a slow dissociation from FimH may be pivotal in the development of effective FimH ligands.

Most of the reported binding-affinity studies are based on enzyme-linked immunosorbent assay (ELISA) or surface plasmon resonance, which analyze the binding affinity of the ligands with the purified recombinant lectin domain of FimH protein as an overly simplified model.[18,22−25] However, it has been shown that mannoside binding affinities are strongly dependent upon the interactions between the lectin and pilin domains of FimH,[26] which is influenced by various conditions, in particular shear stress.[27] In this work, we developed an efficient and reliable flow cytometry method (FCM) for direct assessment of the binding affinity between mannoside derivatives and live *fim*+ *E. coli* 83972. It is based on measurement of the half maximal inhibitory concentration (IC_{50}) of the mannoside ligands against the binding of *fim*+ *E. coli* 83972 to polystyrene microspheres tethering α-D-mannoside.[28−31] Furthermore, we describe the study of the early stage adhesion and biofilm formation by *fim*+ *E. coli* 83972 on silicone surfaces presenting these mannoside derivatives with a wide range of binding affinities to the bacteria. The results clearly reveal the relationship between the mannoside affinity and biofilm formation of *fim*+ *E. coli* 83972. To shed light on the underlying mechanism, we also describe the result of mass spectrometry-based proteomic analysis of the extracellular polymeric substances (EPS) of the biofilms after growth for 48 hours.

2. RESULTS AND DISCUSSION

2.1. Synthesis of a Series of Ortho-Substituted α-Phenyl Mannoside Ligands. Previous reports have shown that the introduction of a phenylene with *o*-CF_3 or *o*-CH_3 group in the glycosidic position greatly enhance the secondary interactions between the mannoside ligands with the "tyrosine

https://dx.doi.org/10.1021/acsami.9b17868
ACS Appl. Mater. Interfaces 2020, 12, 21300−21310

Scheme 1. Overview of the Synthesis of Ortho-Substituted Biphenyl Mannosides[a]

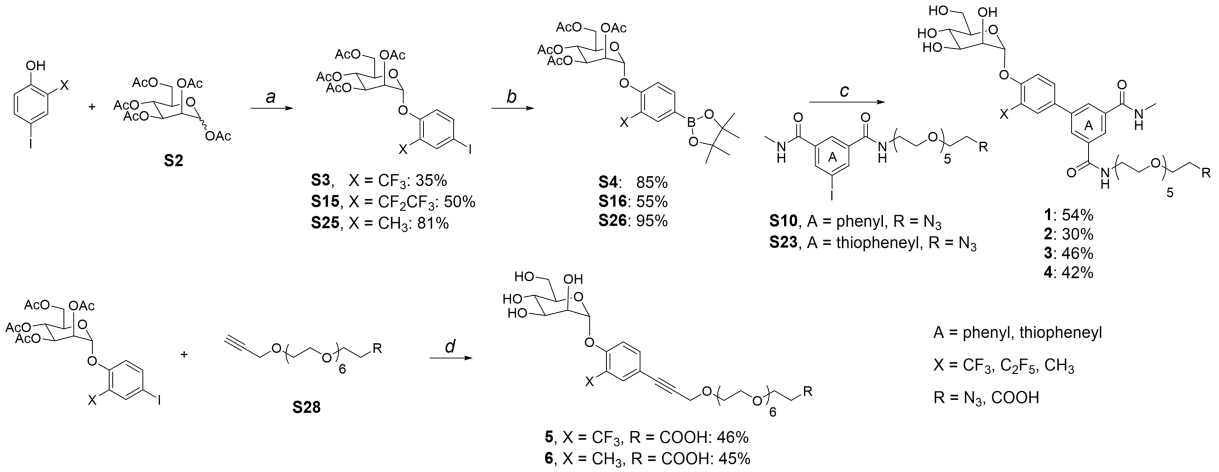

[a]See the Supporting Information for details. Reagents and conditions: (a) BF_3·etherate, DCM, 42 °C, 48 h; (b) bis(pinacolato)diboron, potassium acetate, $PdCl_2$(dppf), DMSO, 80 °C, 12 h; (c) $Pd(PPh)_4$, CsF, THF, 80 °C, 12 h, then NaOMe, MeOH, rt, 12 h; (d) Et_3N, THF, $PdCl_2(PPh_3)_2$, CuI, rt, 4 h.

gate" (Tyr137 and Tyr48) as well as the hydrophobic ridge (Ile13) of FimH, resulting in a substantial improvement of the mannsoide-FimH binding affinity.[18,22] Accordingly, three ortho-substituted analogs bearing $-CF_3$, $-C_2F_5$, and $-CH_3$ on the phenylene ring A shown in Figure 1 were synthesized. Among them, to evaluate the size effect of the ortho-substituents, we prepared the C_2F_5-substited **2** as a new analogue to the reported analogue of the CF_3-substited **1** and the CH_3-substituted **3**,[22] all of them with an oligo(ethylene glycol) linker end-capped with a functional group (COOH or azido) for surface attachment. Moreover, to generate mannoside derivatives with a wide range of binding affinities, we substituted the phenyl ring B with thiopheneyl and alkynyl groups that may have various interactions with Arg98 and Tyr48 of FimH.

Mannoside ligands were prepared by glycosylation of mannoside penta-acetate with 2-substituted-4-iodophenols in the presence of a strong Lewis acid (BF_3 etherate) (Scheme 1).[22] The boronate ester was installed via a Pd-catalyzed coupling reaction. The Suzuki cross-coupling reaction was performed with iodophenyl diamide to give acetyl-protected ortho-substituted biphenyl mannosides, followed by the deprotection under sodium methoxide to give compounds **1**−**4**. Synthesis of the alkynyl mannoside derivatives **5** and **6** followed a similar procedure but proceeded under Sonogashira cross-coupling with alkyne derivatives, thereafter deprotection (Scheme 1).

2.2. Mannoside-Modified TentaGel Polystyrene Microspheres. Flow cytometry (FCM) is a sensitive analytical technique widely used in the evaluation of cellular biochemical and biophysical properties. Host epithelium cells were conventionally used as a substrate to evaluate the FimH-mannoside interaction.[31] However, the heterogeneity from the variations in glycoproteins on the host cell and FimH expression levels and conformation on the bacterial cells, together with the complication of noncovalent interactions between bacteria cells, may significantly interfere with the assay.[32] We established a stable substrate with well-defined surface mannosides for this study by employing 10 μm polystyrene microspheres with alkynyl groups for covalent attachment of the azido-mannosides via click chemistry (Scheme 2). Briefly, 4-pentynoic acid was chlorinated and coupled with 4-(hydroxymethyl)benzoic acid (HMBA) to generate an alkynyl-HMBA linker in 83% yield over two steps. The amino terminated TentaGel polystyrene microspheres were coupled with the alkynyl-HMBA linker in the presence of coupling agents. The azido-functionalized mannoside[9] was attached to the alkynyl-terminated TentaGel polystyrene microspheres via the CuAAC reaction to give the manno-

Scheme 2. Scheme for the Modification of TentaGel Polystyrene Microspheres with Mannoside (PS-Mannoside), and Hydrolysis of PS-Mannoside for LC-MS Quantification

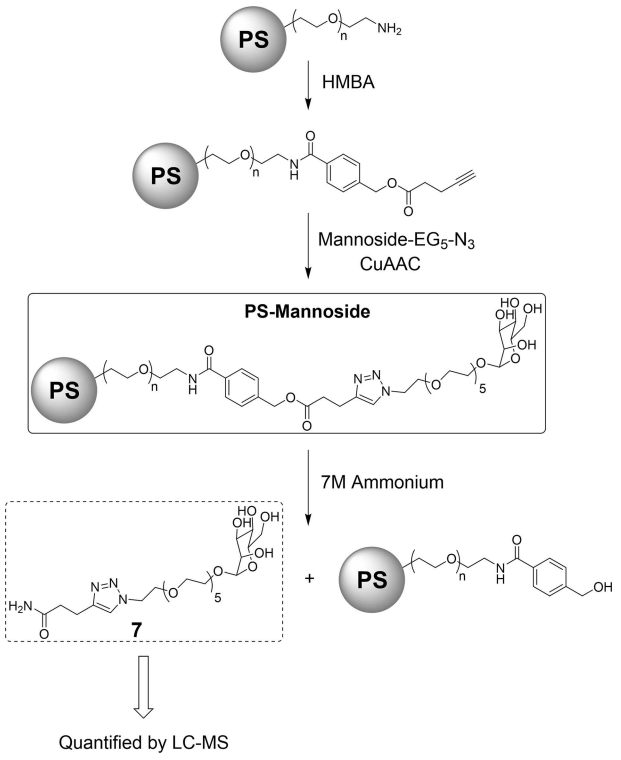

https://dx.doi.org/10.1021/acsami.9b17868
ACS Appl. Mater. Interfaces 2020, 12, 21300−21310

side-modified TentaGel polystyrene microspheres (**PS-Mannoside**).

The **PS-Mannoside** microspheres was analyzed by Fourier transform infrared spectroscopy (FTIR). In Figure 2, the peaks

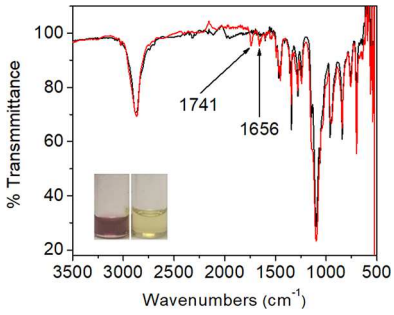

Figure 2. FTIR spectra of the unmodified and modified TentaGel polystyrene microspheres (red line, **PS-Mannoside**; black line, the unmodified TentaGel microspheres). The insets are the images of unmodified amino particles in brownish red (left panel) and **PS-Mannoside** in pale yellow (right panel) after the Kaiser test.

at ~1741 and 1657 cm^{-1}, attributed to the C═O stretching of −COO− and −CONH−, respectively, were observed in **PS-Mannoside**, whereas they were absent in the amino-terminated TentaGel polystyrene microspheres. The Kaiser test also showed the color difference between the unmodified TentaGel polystyrene microspheres (brownish red, Figure 2, left panel) and **PS-Mannoside** (pale yellow, Figure 2, right panel). The microscopic imaging was also employed to examine the morphology of the particles. Compared with the unmodified microspheres (Figure S1a), **PS-Mannoside** remained a similar spherical structure (Figure S1b), with an average size of 13.2 ± 0.4 μm (Figure S2). The zeta potential result was also in agreement with the polarity shift during microsphere functionalization, from 22.0 ± 3.2 mV for the unmodified amino-terminated polystyrene microsphere, to −4.9 ± 0.7 mV for the intermediate, nonpolar alkynyl-modified polystyrene microsphere, and finally to 29.3 ± 4.0 mV for the polar **PS-Mannoside**.

It is challenging to quantify the density of immobilized mannoside ligands on the **PS-Mannoside**. The conventional surface analysis techniques, such as elemental analysis, X-ray photoelectron spectroscopy (XPS), energy-dispersive spectroscopy (EDS), and secondary ion mass spectroscopy (SIMS), analyze only specific elements on the functionalized materials. Therefore, they are not applicable to this study because of the similar elemental composition of mannoside and TentaGel polystyrene microspheres. To circumvent this difficulty, we used LC-MS to quantify the hydrolyzed surface-bound mannoside ligands from the **PS-Mannoside**. An ammonium hydrolysis method was optimized to hydrolyze the ester linkage in **PS-Mannoside** with quantitative conversion (Scheme 2).[33] The resultant mannoside amide (7) was isolated from the microsphere by filtration for LC-MS analysis. The amount of mannoside fragment from **PS-Mannoside** was then quantified against the calibration curve of the mannoside amide (7) standard (mean detector signal vs. concentration, Figure S3). The particle density was determined to be approximately 2 × 10^6 particles/mg and the average mannoside density was (6.80 ± 0.02) × 10^8 mannoside per particle.

2.3. Establishment of Flow Cytometry-Based Binding Affinity Assay. In this setup, the **PS-Mannoside** was used as a substrate to probe the mannoside ligand−*E. coli* 83972 binding affinity through a competitive binding assay. *E. coli* 83972 was

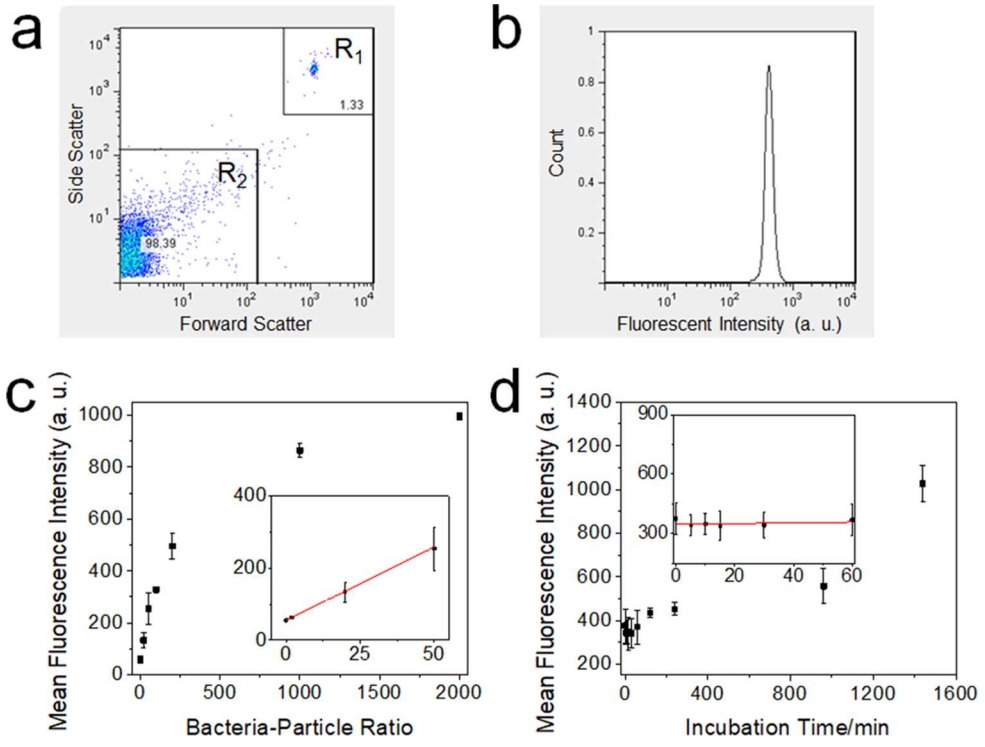

Figure 3. (a) An example of the acquired flow cytometry data plotting the side/forward scatter with region R_1-polystyrene microspheres population and region R_2-*E. coli* 83972 population, (b) histogram of the MFI of the bacteria adhered microspheres, and optimization of (c) the bacterium to particle ratio and (d) incubation time. Red lines in (c) and (d) are linear fitting curves.

https://dx.doi.org/10.1021/acsami.9b17868
ACS Appl. Mater. Interfaces 2020, 12, 21300−21310

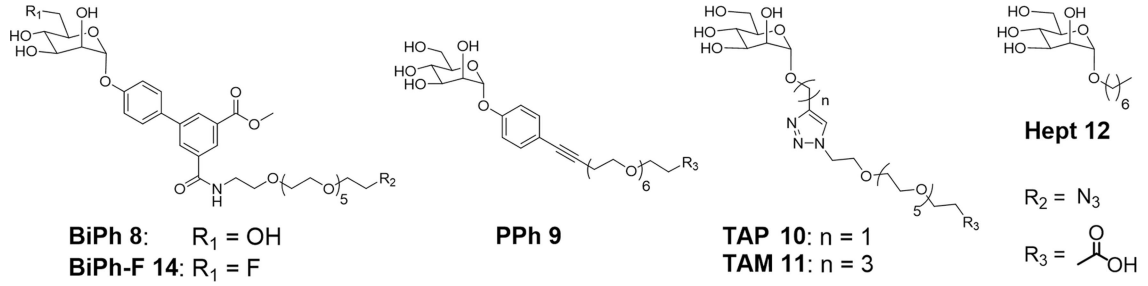

Figure 4. Structures of mannoside ligands **8**−**14**.

fluorescently labeled with tetrazolium salt 5-cyano-2,3-ditolyltetrazolium chloride (CTC) (Figure S4) that can be identified by flow cytometry.[34]

To analyze each individual component in the binding affinity assay, we recorded three key parameters: (a) planktonic bacterial number; (b) bacteria adhered particle number; and (c) bacteria-free particle number. The forward/side scatter detection differentiated particles from planktonic bacteria, and the mean fluorescence intensity (MFI) was used as an orthogonal detection to distinguish bacteria adhered particles from bacteria-free particles. The above-mentioned components were quantified individually with high accuracy by collecting tens of thousands of events as data points.

Two "gates" (designated as R_1 and R_2 in Figure 3a) were established in forward/side scatter to differentiate the recorded events into the corresponding groups. As shown in a representative calibration sample of *E. coli* 83972 and **PS-Mannoside** mixture, region R_1 contained the polystyrene microsphere population, including the bacteria adhered particles. Region R_2 included all planktonic bacteria. Despite of their tiny size, bacteria population had a wide range size distribution because of inherent heterogeneity and asymmetry morphology as well as small number of aggregates, thus occupying a major area in the lower quadrant of logarithmic scatter plot. Figure 3b shows the histogram of the MFI of the bacteria adhered particles.

The 10 μm polystyrene microspheres resemble the epithelial cells with multidentate mannosylated surface. The significantly larger surface area of the polystyrene microsphere comparing to a bacterial cell enables the accommodation of multiple bacteria on its surface, which can be easily distinguished from the planktonic bacterial cells (Figure 3a). For ligand exchange to occur, it is desirable to have excess **PS-Mannoside** to minimize the population of planktonic bacteria in the system prior to the introduction of competing FimH ligands. However, it is equally important to maintain a sufficient density of bacteria per particle for reliable fluorescence detection. Thus, we optimized the bacterium to particle ratio varying from 2:1 to 2000:1. As shown in Figure 3c, the mean fluorescent intensity (MFI) of the bacteria adherent microspheres increased with the increasing the bacterium to particle ratio, rapidly at low bacterium to particle ratios and slowly at high bacterium to particle ratios, and nearly plateaued at the end. Microscopic images of the bacterium−particle complex also indicated the functionalized microsphere surface tended to aggregate at high bacterium to particles ratio (Figure S5). Therefore, we chose a bacterium to particle ratio of 50:1 for our following studies. In addition, the bacteria-particle suspension was incubated for various times between 0 to 24 h to assess the stability of *E. coli* 83972 adhesion on the **PS-Mannoside**. As indicated in Figure 3d, the MFI of bacteria adhered particles remained constant within 1 h (red line) and subsequently started to increase, which was likely due to bacterial growth over the incubation period. Therefore, an incubation time of 30 min was used for the following studies.

2.4. FCM-Based Inhibition Assay for Screening FimH Ligands. To evaluate the binding affinity of different FimH ligands, we added the mannoside derivatives into the bacteria−particle mixed suspension with an increasing concentration. The competition binding with the mannoside derivatives resulting in the dissociation of the bacterium−particle complex, with a concomitant decrease in the microsphere fluorescence intensity on the particles. On this basis, the half maximal inhibitory concentration (IC_{50}) is an index of the binding affinity of mannoside ligands toward the FimH lectin on the bacteria, which was derived from a sigmoid inhibition curve (MFI vs. log[ligand]). To compare our result with those documented in the literature, we chose a reported high-affinity ligand, *n*-heptyl α-D-mannopyranoside **Hept**, as a reference compound. Thirteen potential FimH ligands (Figures 1and 4) were evaluated with this high-throughput flow cytometry assay. The IC_{50} values (Table 1) of the evaluated mannoside ligands followed this order: **BiPh−CF_3** (**1**) < **BiPh−CH_3** (**3**) < **BiPh−C_2F_5** (**2**) < **BiPh−CF_3-TP** (**4**) < **PPh−CF_3** (**5**) < **PPh−CH_3** (**6**) < **BiPh** (**8**) < **PPh** (**9**) < **Hept** (**12**) < **TAP** (**10**) < **TAM** (**11**). As we expected, the analogous fluorinated biphenyl mannoside **BiPh-F** (**14**) showed no inhibitory effect even with a concentration of up to 10 mM, indicating that the

Table 1. List of the IC_{50} and rIC_{50} Values for the Mannoside Ligands 1−14 to *fim*+ *E. coli* 83972 as a Measure of Their Binding Affinity[a]

	mannoside	IC_{50} [μM]	rIC_{50}[b]
1	**BiPh−CF_3**	0.098 ± 0.040	0.0055
2	**BiPh−C_2F_5**	0.26 ± 0.17	0.015
3	**BiPh−CH_3**	0.15 ± 0.04	0.0084
4	**BiPh−CF_3-TP**	0.32 ± 0.17	0.018
5	**PPh−CF_3**	0.79 ± 0.22	0.044
6	**PPh−CH_3**	1.46 ± 0.49	0.082
8	**BiPh**	4.5 ± 1.3	0.25
9	**PPh**	6.9 ± 3.0	0.39
10	**TAP**[10]	959 ± 417	53.9
11	**TAM**[10]	8340 ± 3084	468.5
12	**Hept**	18 ± 10	1.00
13	**D-(+)-Galactose**	N.A.	N.A.
14	**BiPh-F**[10]	N.A.	N.A.

[a]The corresponding sigmoid inhibition curves of each mannoside ligand (Figures 1 and 4) are provided in the Supporting Information in Figure S6. [b]Relative IC_{50} (rIC_{50}) were normalized to **Hept 12** (reference compound).

https://dx.doi.org/10.1021/acsami.9b17868
ACS Appl. Mater. Interfaces 2020, 12, 21300−21310

structural integrity of mannoside is pivotal for the binding interaction with the FimH binding site, which could not be substituted by the glycosidic biphenyl moiety. The negative control compound, **D-galactose** (**13**) did not exhibit an inhibitory effect with a concentration of up to 10 mM. The IC_{50} of the reference compound **Hept** (**12**) was in a low μM range (18 ± 10 μM), as a medium potency ligand. Remarkably, all the biphenyl and alkynylphenyl derivatives showed higher binding affinity, with **BiPh−CF_3** (**1**) as the most potent ligand (IC_{50} = 0.098 ± 0.040 μM). The hydrophobic ortho-substitution improved the inhibitory potency in the order of CF_3 > CH_3 > C_2F_5. This result is in agreement with the reported analogues of **1** and **3**, attributed to the hydrophobic interactions with the FimH hydrophobic ridge (Ile13, Ile52) and the "tyrosine gate" enable further enhancement of the binding.[22] These interactions are the largest for ligands **1**−**3** with the largest hydrophobic surface area compared to the other ligands. The larger size C_2F_5 substitution in **2** reduced the binding affinity by 3 times compared to **1**, attributable to the increased steric hindrance. Although thiopheneyl diamide and alkynylphenyl mannoside derivatives were reported to be promising candidates as the FimH inhibitor,[22,25] the thiopheneyl (**4**) and alkynyl (**5** and **6**) analogues exhibited a weaker inhibitory effect than **BiPh−CF_3** (**1**). The substitution of phenyl group with thiopheneyl group or alkynyl group led to a more than 3-fold decrease in binding affinity, suggesting the presence of phenyl analog is crucial for $\pi-\pi$ stacking with the Tyr48 residue of FimH. In summary, contribution to the binding affinity follows the order of phenyl moiety > ortho-substitution > heterocyclic substitution in the terminal biphenyl ring. Significantly, ligands **1**−**6** were up to 45 times more potent than the four mannosides (**8**−**11**) used in our previous studies.[9−11] All these mannosides exhibit a wide range of binding affinities (over 5 orders of magnitudes in IC) to the bacteria, allowing us to investigate the role of the ligand binding affinity on the biofilm formation.

2.5. Formation of *E. coli* 83972 Biofilms on Mannoside-Modified Silicone Surfaces. To explore the underlying relationship between the mannoside binding affnity and the formation of *fim*+ *E. coli* 83972 biofilms, we cultured the bacteria on the silicone surfaces modified with a series of mannoside ligands exhibiting a broad range of binding affinities. The mannoside **2** was chosen as a representative of **2**−**4**, because of the similarity in structure and binding affinity. The negative control ligand **14** was not used in the biofilm formation test, nor the reference ligand **12** lacking an active functional group, e.g. azido or carboxyl group, for covalent attachment. As shown in Figure 5, after a 48 h continuous static culture of *fim*+ *E. coli* 83972, the surface biofilm coverage followed this order: **BiPh−CF_3(1)** > **BiPh−C_2F_5(2)** > **PPh−CF_3** (**5**) ≈ **PPh−CH_3(6)** ≈ **BiPh** (**8**) > **PPh** (**9**) > **TAP** (**10**) > **TAM** (**11**). This order was consistent with the aforementioned trend in the binding affinity of FimH ligands.

Because the **BiPh−CF_3** (**1**) modified surface exhibited the highest potency to form dense biofilms, the *fim*+ *E. coli* 83972 biofilms on the corresponding surface were further investigated. As shown in Figure 6a, a densely packed biofilm was formed on the **BiPh−CF_3** presenting surface. Moreover, it was found that the bacteria were embedded in a large amount of lamellar and chunk matrix as the extracellular polymeric substances (EPS, Figure 6b) that were formed during biofilm formation and were responsible to the interbacterial binding.[35,36] The thickness of the biofilms on the **BiPh−CF_3** (**1**)

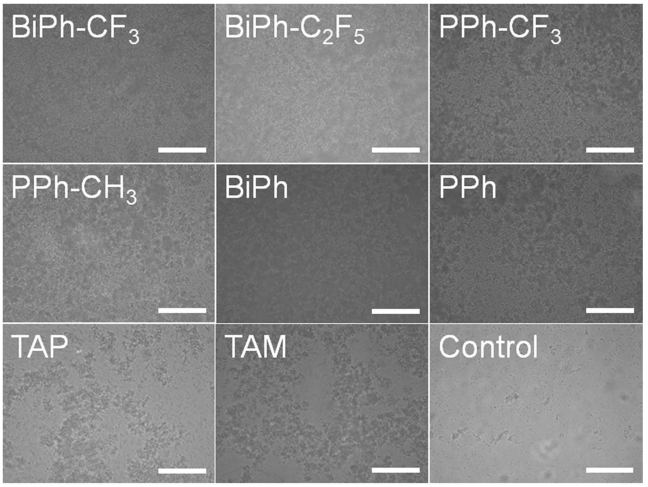

Figure 5. Representative reflected bright-field images of *fim*+ *E. coli* 83972 biofilms formed after 48 h of continuous static culture on the indicated mannoside modified surfaces. The surface was incubated with *fim*+ *E. coli* 83972 culture (1×10^8 CFU/mL, $[OD]_{600}$ = 0.25) in 1 mL of fresh LB broth, followed by detachment of the loosely bounded bacteria cells. Scale bar: 50 μm. The control group was the silicone surface without mannoside modification.

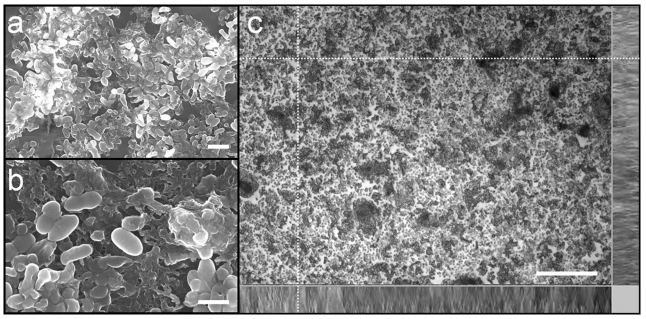

Figure 6. (a, b) SEM and (c) reflected bright-field images of a biofilm of *fim*+ *E. coli* 83972 formed after 48 h of continuous static culture on a **BiPh−CF_3** presenting surface. Scale bars are (a) 2, (b) 1, and (c) 50 μm, respectively. Right and bottom margins in c represent the cross-section image acquired across the vertical and horizontal dot lines, with a *Z*-scan step of 1.5 μm and a range Z_0 of ±20.0 μm.

presenting surface was also evaluated via optical microscopy using the Z-scan technique, and the thickest region was approximately 20 μm (Figure 6c).

Collectively, the FimH binding affinity of mannosides and the coverage of biofilms (Figure 7a) show a strong correlation, with the correlation coefficient (r) being −0.89 (Figure 7b). It also indicates that the strong mannoside ligands determine the early stage adhesion and biofilm formation of *fim*+ *E. coli* 83972.

2.6. Proteomic Composition of *fim*+ *E. coli* 83972 Biofilm Matrices on Mannoside-Modified Silicone Surfaces. To shed light on the mechanism underlying the observed correlation between mannoside binding affinity with bacterial adhesion and biofilm formation, we detached *fim*+ *E. coli* 83972 biofilm from various mannoside surfaces and the EPS proteins were extracted and analyzed by shot-gun proteomics using mass spectrometry. In this study, substrates modified with the mannosides **1**, **3**, **5**, **6**, **8**, **9**, and **10** with binding affinity (IC_{50}) to *fim*+ *E. coli* 83972 over 4 orders of magnitude were incubated in the culture of *fim*+ *E. coli* 83972

https://dx.doi.org/10.1021/acsami.9b17868
ACS Appl. Mater. Interfaces 2020, 12, 21300−21310

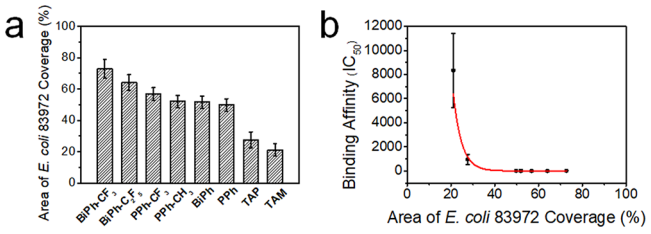

Figure 7. (a) Bar chart to compare the *fim+ E. coli* 83972 biofilm coverage after 48 h continuous static culture on a series of mannoside surfaces. (b) Scatter diagram of binding affinity (IC_{50}) and the area of *fim+ E. coli* 83972 coverage (%). The red line is an exponential fitting trend line ($y = 0.09508 + 1.541 \times 10^6\ e^{-0.2603x}$, $R^2 = 0.8$) that reflects the correlation between the binding affinity and biofilm coverage.

for 48 h. The biofilms were detached by treatment with EDTA and the bacteria were removed by centrifugation. EPS proteins in the supernatant were identified, and the number of protein groups was listed in Table 2. Among all the identified proteins,

Table 2. Number of Protein Groups Identified in the Biofilm Matrix Grown on Substrates Modified with Mannoside Ligands

entry	compound	protein groups
1	**BiPh−CF_3**	954 ± 7
3	**BiPh−CH_3**	918 ± 7
5	**PPh−CF_3**	1155 ± 12
6	**PPh−CH_3**	1080 ± 18
8	**BiPh**	1220 ± 22
9	**PPh**	908 ± 19
10	**TAP**	716 ± 13

550 protein groups were identified in all samples, and their molecular function classification[37] was shown in Figure 8a. Among them, 61 protein groups showed more than 2-fold changes among various surfaces (protein profile heatmap in Figure S7), and their molecular function classification[37] is shown in Figure 8b. These two groups of proteins exhibited a similar distribution in molecular functions. A complete list of the protein groups that were identified, and that exhibited more than 2-fold changes within samples are provided in the Supporting Information. Furthermore, proteins that were only present in one sample and not in other samples were also identified. This result indicated that the binding affinity of the mannoside presented on the surface significantly affected the proteomic composition of the biofilm matrix (EPS). Our results showed that surfaces presenting mannosides with a higher affinity to *fim+ E. coli* 83972 greatly increased the long-term stability of the biofilms and their efficiency for inhibiting the colonization by pathogens.[9,10] The substantial difference in the EPS protein compositions determined on surfaces presenting mannosides with a wide range of binding affinity indicates that the initial mannoside-FimH binding might trigger the production and secretion of the EPS whose amount and composition may depend on the strength of the mannoside-FimH binding. The association of bacteria-surface interactions with the EPS secretion and other biofilm formation processes has been implicated.[36,38,39] Further investigation is required to shed light on the potential and yet unannotated functions of the EPS proteins related to biofilm formation and bacterial interference, which is a subject under active investigation by our laboratories.

3. CONCLUSION

In summary, we synthesized a series of ortho-substituted α-phenyl mannoside derivatives with a wide range of binding affinity to *fim+ E. coli* 83972. A novel FCM based method was established to evaluate the binding affinity between mannoside ligands and the bacteria. We demonstrated a strong correlation between the binding affinities of immobilized mannoside derivatives and the early stage adhesion and biofilm formation of *fim+ E. coli* 83972. Mass spectrometry based proteomic analysis indicated a substantial difference in the proteome of the extracellular polymeric substance (EPS) secreted by biofilms on different mannoside surfaces, which might be related to the biofilm formation and stability.

4. MATERIALS AND METHODS

4.1. Synthesis of Mannosides Derivatives. The synthesis of mannoside derivatives, **BiPh**, **PPh**, **TAM**, **TAP**, and **BiPh-F** was described in detail previously.[10] The mannoside derivative **Hept** was synthesized as previously described.[21] The synthesis of mannoside derivatives **BiPh-CF_3**, **BiPh-C_2F_5**, **BiPh-CF_3-TP**, **PPh-CF_3**, and **PPh-CH_3** is reported in the supplementary content. D-(+)-Galactose was obtained from Sigma-Aldrich.

4.2. Synthesis of G5 PAMAM-Mannoside. *Synthesis of G5 PAMAM-Mannoside by Amidation.* To conjugate the mannoside with G5 PAMAM dendrimer, we first activated 2.94 μmol mannosides (**PPh**, **BiPh**, **PPh−CF_3**, **PPh−CH_3**, **TAM**, and **TAP**) by sulfo-*N*-hydroxysuccinimide (sulfo-NHS, 3.2 mg, 14.7 μmol, Thermo Fisher Scientific, USA) and 1-ethyl-3-(3-dimethylaminopropyl) carbodiimide hydrochloride (EDC·HCl, 5.7 mg, 29.4 μmol, Thermo Fisher Scientific, USA) in 500 μL of ultrapure water at 25 °C for 15 min. G5 PAMAM dendrimer (5.4 mg, 0.21 μmol, Sigma-Aldrich, USA) in 100 μL of ultrapure water was added to the activated mannoside mixture and shaken at 1500 rpm and 25 °C for 12 h on a Scilogex MX-M shaker. The resulting product was purified by Amicon Ultra-4 mL Centrifugal Filters (3K MWCO, EMD Millipore, USA) at 4000 rpm and 16 °C for 40 min. Three milliliters of ultrapure water was

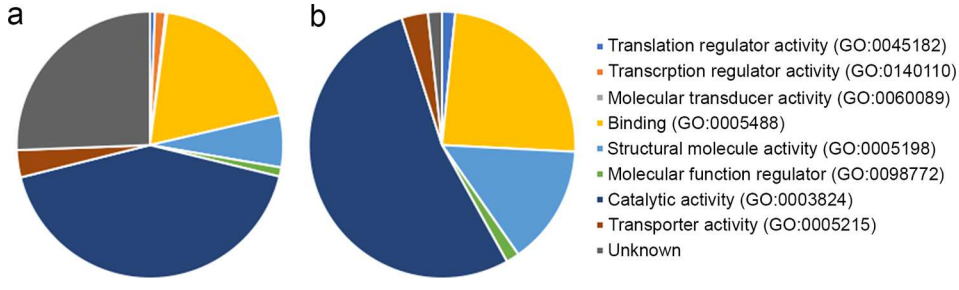

Figure 8. Molecular function classification of (a) protein groups identified in all the *fim+ E. coli* 83972 biofilm EPS, and (b) protein groups exhibiting more than 2-fold changes in the *E. coli* 83972 biofilm matrices grown on a series of mannoside surfaces listed in Table 2.

https://dx.doi.org/10.1021/acsami.9b17868
ACS Appl. Mater. Interfaces 2020, 12, 21300−21310

subsequently added to the centrifugal filter for wash. The wash-centrifugation cycle was repeated five times. The G5 PAMAM-mannoside codendrimers were recovered as white powder after lyophilization.

Synthesis of G5 PAMAM-Mannoside Codendrimers by Click Chemistry. Pentynoic acid (0.3 mg, 2.94 μmol), 2.94 μmol mannosides (**BiPh-CF_3**, **BiPh-C_2F_5**, **BiPh-CF_3-TP**, and **BiPh-CH_3**), $CuSO_4$ (0.1 mg, 0.625 μmol), tris(triazolyl)-tetraoligoethylene glycol ligand (0.5 mg, 0.63 μmol), and sodium ascorbate (2.0 mg, 10 μmol) were dissolved in 400 μL of ultrapure water and shaken at 1500 rpm in an anaerobic chamber ($[O_2]$ < 0.1 ppm) at 25 °C for 6 h. Afterward, sulfo-NHS (3.2 mg, 14.7 μmol) and EDC·HCl (5.7 mg, 29.4 μmol) in 100 μL of ultrapure water were added to the mixture for 15 min to active the carboxylic groups. G5 PAMAM dendrimer (5.4 mg, 0.21 μmol) in 100 μL of ultrapure water was slowly added into the mixture and vigorously shaken at 25 °C for 12 h. After completion, 200 μL of 10 mM pentasodium DTPA (Sigma-Aldrich, USA) was added to remove the copper ions. The resulting product was purified by Amicon Ultra-4 mL Centrifugal Filters (3K MWCO) at 16 °C and 4000 rpm for 40 min. Three milliliters of ultrapure water was subsequently added to the centrifugal filter for wash. The wash–centrifugation cycle was repeated five times. The G5 PAMAM-mannoside codendrimers were recovered as white powder after lyophilization.

4.3. Preparation of Mannoside-Modified TentaGel Polystyrene Microspheres. *Preparation of Alkynyl-Modified TentaGel Polystyrene Microspheres.* 1-Hydroxybenzo-triazole (23 mg, 0.2 mmol), EDC·HCl (38 mg, 0.2 mmol), and 4-((pent-4-ynoyloxy)-methyl)benzoic acid (46 mg, 0.2 mmol) were dissolved in 1 mL 1-methyl-2-pyrrolidinone and shaken at 1500 rpm and 25 °C for 15 min. Afterward, 100 mg of amino-terminated TentaGel microspheres (10 μm) were added and kept stirring at 25 °C for 4 h. After completion, the reaction was quenched by 2 mL of ultrapure water. The resulting particles were sonicated for 5 min and centrifuged at 10 000 × g for 5 min. The wash–centrifugation cycle was repeated for four times with a washing solution of EtOH/H_2O (1:1). The product was resuspended in 1 mL of ultrapure water and stored at 4 °C.

*Preparation of Mannoside (**7**)-Modified TentaGel Polystyrene Microspheres.* Alkynyl-modified TentaGel microspheres (20 mg), mannoside **7** (15 mg, 0.01 mmol), $Cu(OAC)_2$ (5 mg, 0.0187 mmol), tris(triazolyl)-tetraethylene glycol mannoside (20 mg, 0.026 mmol),[9] and sodium ascorbate (10 mg, 0.05 mmol) were dissolved in 1 mL MeOH/H_2O (4:1) and shaken at 1500 rpm and 25 °C for 20 h in anaerobic chamber ($[O_2]$ < 0.1 ppm). The particles were filtered by 10.0 μm 25 mm polycarbonate (PCTE) membrane filters (SterliTech, USA) to remove the smaller size impurities. Water and ethanol were added to wash the particles. The particles were dried in a vacuum furnace overnight. Ultrapure water was added to adjust the particle concentration to 100 mg/mL (~2 × 10^8 particles/mL) and stored at 4 °C.

4.4. Characterization of Mannoside-Modified TentaGel Polystyrene Microspheres. *Ammonium Cleavage.* Mannoside fragment (**7**) was released from the **PS-Mannoside** in a 7 M ammonia methanol solution for 24 h with magnetic stirring at 1500 rpm at 25 °C. The particle concentration was adjusted to 0.5 mg/mL in methanol. After completion, the supernatant was filtrated by a 0.22 μm PTFE syringe filter (EMD Millipore, USA) for LC-MS analysis.

LC-MS Analysis. A 100 μL **PS-Mannoside** hydrolysis solution was diluted five times in methanol and 1 μL of the diluted sample was injected. All the mass analysis was conducted on Thermo Finnigan LCQ Deca XP Plus LC/MS system equipped with a C18 column (Kinetex XB-C18, Phenomenex, USA) in gradient elution (10–95% Acetonitrile in H_2O, 12 min). Each sample was analyzed in duplicate to calculate the concentration of mannoside fragment (**7**).

4.5. Bacterial Strains. The strain of *Escherichia coli* 83972 expressing type 1 fimbriae was kindly given by Prof. Barbara Trautner at Baylor College of Medicine. For all the bacterial associated experiments, a single colony was inoculated in 50 mL of Lysogeny Broth (LB, Becton-Dickinson, USA) media containing 20 mg/mL chloramphenicol for the positive selection of *fim*+ *E. coli* 83972. Bacterial cultures were grown until log phase and diluted in fresh LB media. The optical density at 600 nm (OD_{600}) for each bacterial culture was adjusted to 0.25, corresponding to 1 × 10^8 CFU/mL.

4.6. Optimization of Bacteria–Particle Incubation Condition. To optimize the bacterium to particle ratio, we mixed 5-cyano 2,3-ditoyl tetrazolium chloride (CTC, Cayman Chemical, USA) labeled *fim*+ *E. coli* 83972 with the **PS-Mannoside** at bacterium to particle ratios of 2:1, 20:1, 50:1, 200:1, 1000:1, and 2000:1. Accordingly, the *fim*+ *E. coli* 83972 suspension was diluted to 4 × 10^6, 4 × 10^7, 1 × 10^8, 4 × 10^8, 2 × 10^9, and 4 × 10^9 CFU/mL in phosphate buffered saline (PBS, Sigma-Aldrich, USA). One milliliter of the above *fim*+ *E. coli* 83972 solutions was mixed with 200 μL of **PS-Mannoside** (2 × 10^6 particles/mL), respectively. To optimize the incubation time, we monitored the *fim*+ *E. coli* 83972 and **PS-Mannoside** mixture monitored from 0–24 h.

4.7. FCM-Based Inhibition Assay for Screening FimH Ligands. *Sample Preparation.* The particle stock solution (100 mg/mL, ~ 2 × 10^8 particles/mL) was diluted into a concentration of 5 mg/mL (approximately 1 × 10^7 particles/mL) with ultrapure water and homogenized by sonication for 10 min. For the bacteria-mannoside binding studies, 1 mL of fluorescent labeled 10^8 CFU/mL *fim*+ *E. coli* 83972 suspension (maximum emission wavelength, λ_{em}= 630 nm) were mixed with 200 μL of functionalized particle suspension (2 × 10^6 particles; bacteria-particle ratio = 50:1), thereafter transferred into a 5 mL round-bottom FCM polystyrene test tube (BD Falcon, Becton Dickinson, USA). The mixture was shaken at 200 rpm and 25 °C for 30 min.

Flow Cytometry Analysis. FCM analysis was performed on BD FACS Calibur (Becton Dickinson, USA) equipped with an argon laser (15 mW, 488 nm). The recorded parameters include forward scatter (FSC), side scatter (SSC), and fluorescence 3-Height (FL3). CTC red fluorescence was measured in the FL-3 channel (band-pass filter 670 nm, named CTC intensity). The CELLQuest software (version 4.0, Becton Dickinson, USA) was utilized for the data acquisition. The acquired data was then analyzed by FlowJo software (version 8.0, FlowJo LLC., USA). Four reference samples were applied for the parameter calibration: (a) the 10 μm unmodified TentaGel microsphere suspension was exploited to set the voltage and the gain of the photomultiplier tube (PMT) for the optimal distinguishing planktonic bacteria from functionalized particles; (b) the non-fluorescent *fim*+ *E. coli* 83972 suspension was employed to tune the FL-3 channel gain; (c) the CTC dyed fluorescent *fim*+ *E. coli* 83972 suspension was utilized to regulate the FL-3 channel PMT for amplifying contrast between the nonfluorescent events and the CTC fluorescent events; (d) the sterile PBS was taken to set the threshold value for minimizing the system noise. All parameters were fixed throughout the whole data acquisition process. At least 1000 particle events were recorded for each sample.

The half maximal inhibitory concentration (IC_{50}) is an index of the binding affinity of mannoside ligands toward FimH lectin, which was derived from a sigmoid inhibition curve (mean fluorescence intensity (MFI) vs. log[ligand]).

4.8. Biofilm Formation of *fim*+ *E. coli* 83972 on Silicone Surfaces. The preparation of mannoside modified silicone surfaces was reported previously with modification.[11] A 1 cm × 1 cm silicone surface was oxidized by using CO_2 plasma (Basic Plasma Cleaner, Model PDC-32G, 100 W, Harrick Plasma, USA). The as-synthesized G5 PAMAM-mannoside (1 mg/mL) was added immediately to the oxidized polydimethylsiloxane (PDMS, Sylgard 184, Dow Corning, USA) surface, which was statically incubated for 1 h at 25 °C. Thereafter, the resulting surface was rinsed with ultrapure water and dried with a flow of nitrogen.

Subsequently, the silicone surface modified with G5 PAMAM-mannoside was statically incubated with 1 mL of *fim*+ *E. coli* 83972 suspension (~1 × 10^8 CFU/mL) in fresh LB media supplied with chloramphenicol (20 μg/mL) at 37 °C for 48 h. Eventually, the surface was placed in a sterile culture plate and washed with PBS three times (*Note: the plate was gently shaken in the back-and-forth motions on top of a clean bench in the biological safety hood to remove loosely adhered or planktonic bacteria*). The adhered bacteria on the surface were later

https://dx.doi.org/10.1021/acsami.9b17868
ACS Appl. Mater. Interfaces 2020, 12, 21300–21310

observed in a Nikon 80i Microscope by using a 40× objective and fluorescence microscopy with a TRTIC filter, altogether with a CoolSnap HQ2 camera (Photometrics, USA). NIS Elements microscope imaging software (version 4.00, Nikon Instruments, USA) was adopted for both image acquisition and analysis.

4.9. Scanning Electron Microscopy (SEM). The samples were successively fixed with a 2.5% glutaraldehyde solution (Sigma-Aldrich, USA) at 4 °C for 12 h and a 1% OsO_4 solution (Sigma-Aldrich, USA) for 6 h at 25 °C. Afterward, the samples were rinsed with ultrapure water, dehydrated with a series of ethanol solutions (25%, 50%, 75%, 90%, and 100%), and immersed in *t*-butanol. Finally, the samples were lyophilized by using freeze-drier (Scanvac CoolSafe 110−4, LaboGene, USA), sputter-coated with 8 nm of platinum (Hummer 6.2 Sputter System, Anatech, USA), and imaged by FE-SEM (LEO, model 1525, Zeiss, Germany) at an accelerating voltage of 10 kV.

4.10. Z-Series Acquisition (Z-scan). The *fim+ E. coli* 83972 biofilms were formed on the **BiPh−CF_3** presenting surface after 48 h continuous static culture and were fixed with a 2.5% glutaraldehyde solution for 12 h at 4 °C. The Z-scan images were acquired by a Nikon microscope using 40× objective and CoolSnap HQ2 camera, with a Z-scan step of 1.5 μm and a range Z_0 of ±20.0 μm. NIS Elements microscope imaging software was adopted for both image acquisition and analysis.

4.11. Proteomic Sample Preparation. The substrates were incubated in 2 mL of 0.5% EDTA in PBS at 4 °C for 2 h. The solution was collected into a 5 mL tube on ice. The substrates were washed with cold PBS twice and the wash solution was combined into the tube. After centrifugation at 5000 rpm at 5 °C for 5 min, the supernatant was transferred into an Amicon ultra-4 mL centrifugal filter (MWCO 3K) and centrifuged at 4500 rpm at 5 °C for 40 min. After washing for 5 times, the solution was transferred into a sterile 1.5 mL Eppendorf tube. The samples were heated at 90 °C for 30 min, and after cooling, MS-grade trypsin (Thermo Fisher Scientific, USA, Trypsin: sample proteins = 1:50) was added and incubated at 37 °C overnight. The samples were cleaned up using C-18 Ziptip and dissolved in a 0.1% formic acid solution.

4.12. LC-MS. The LC-MS analysis was performed using the Bruker's timsTOF Pro equipped with a NanoElute LC system. The peptide samples were loaded onto an in-house packed column (70 μm x 7 cm, 1.9 μm ReproSil-Pur C18 particle (Dr. Maisch GmbH, Germany), column temperature 20 °C) followed by an 80 min gradient separation. Buffer A (0.1% formic acid in water) and buffer B (0.1% formic acid in ACN) were used as the mobile phases. The gradient included 71 min from 2% B to 25% B and 9 min to 37% B followed by washing with 90% B. Each sample was analyzed in triplicates. The eluted peptides from the columns were sprayed using the CaptiveSpray method into a capillary transfer tube followed by passing through the trapped ion mobility (tims) device and analyzed by a quadrupole time-of-flight (Q-TOF) analyzer. The electrospray voltage was 1.4 kV, and the ion transfer tube temperature was 180 °C. Paralle accumulation serial fragmentation (PASEF) method was employed for data acquisition. Briefly, the full MS scans were acquired over the m/z range of 150−1700. The target intensity value was 2.00×10^5 with a threshold of 2500. A fixed cycle time was set to 1.2 s, and dynamic exclusion duration was 0.4 min with ±0.015 amu tolerance. Only peaks with charge state ≥2 were selected for sequencing and fragmented with a normalized collision energy of 42 eV.

4.13. Proteomic Data Analysis. Database searching was carried out in Peaks Studio 8.5 (Bioinformatics Solutions Inc., Canada). UniProt-SwissProt *E. coli* database (updated on 01/31/2018, 23038 entries.) was used for database searching. Database searching against the corresponding decoy database was also performed to evaluate the false discovery rate (FDR) of peptide identification. The database searching parameters included up to two missed cleavages allowed for full tryptic digestion, precursor ion mass tolerance of 50 ppm, product ion mass tolerance of 0.05 m/z units. The result from each run was filtered with the peptide confidence value with a false discovery rate (FDR) of less than 1%. On the protein level, the minimal number of peptides is 1 for each protein. Additionally, protein grouping was enabled. Accordingly, if the multiple proteins were identified from the same peptides, these proteins were considered as one protein group. Label free quantification was performed with normalization to total ion counts using Peaks Studio 8.5. The results were filtered with peptides identified in all triplicates for each sample, and proteins with at least 1 unique peptide and an FDR of <1%.

To identify proteins that are present in all samples, R script was written to compare data files exported from Peaks Studio proteomic data analysis software by extracting proteins that were overlapped in all of the files. The R script is available upon request.

Protein classification by molecular function was achieved using the PANTHER classification system[37] (http://pantherdb.org).

All MS data were deposited to the Texas Data Repository and available for download (10.18738/T8/0UFTCA).

4.14. Statistical Analysis. Data are provided as mean ± SD. The IC_{50} analysis of FimH-mannoside binding was performed using GraphPad Prism (Version 6.0, GraphPad Software, Inc., USA) in a dose−response model.

■ ASSOCIATED CONTENT

Supporting Information

The Supporting Information is available free of charge at https://pubs.acs.org/doi/10.1021/acsami.9b17868.

Synthesis of mannoside derivatives; functionalization of TentaGel polystyrenemicrospheres; bacterial fluorescence staining; flow cytometry assay; proteins identified in the biofilm matrices; and copies of ^1H, ^{13}C, ^{19}F, and 2D NMR spectra (PDF)

Lists of proteins identified in all triplicates of the *E. coli* 83972 biofilm matrixes grown on various surfaces (XLSX)

■ AUTHOR INFORMATION

Corresponding Authors

Chengzhi Cai − *Department of Chemistry, University of Houston, Houston, Texas 77204, United States;* orcid.org/0000-0001-9800-7769; Email: cai@uh.edu

Guoting Qin − *College of Optometry, University of Houston, Houston, Texas 77204, United States;* orcid.org/0000-0001-8916-6311; Email: gqin@central.uh.edu

Authors

Zhiling Zhu − *Department of Chemistry, University of Houston, Houston, Texas 77204, United States; College of Materials Science and Engineering, Qingdao University of Science and Technology, Qingdao, Shandong 266042, China;* orcid.org/0000-0003-3878-0391

Yanxin Chen − *Department of Chemistry, University of Houston, Houston, Texas 77204, United States;* orcid.org/0000-0002-5853-9135

Siheng Li − *Department of Chemistry, University of Houston, Houston, Texas 77204, United States;* orcid.org/0000-0001-9582-3568

Hong Lin − *Department of Department of Computer and Mathematical Sciences, University of Houston-Downtown, Houston, Texas 77002, United States;* orcid.org/0000-0003-1827-5507

Complete contact information is available at: https://pubs.acs.org/10.1021/acsami.9b17868

Notes

The authors declare no competing financial interest.

https://dx.doi.org/10.1021/acsami.9b17868
ACS Appl. Mater. Interfaces 2020, 12, 21300−21310

■ ACKNOWLEDGMENTS

This work is supported by the National Science Foundation of the United States to CC (DMR-1508722), National Natural Science Foundation of China to ZZ (No. 31800800).

■ REFERENCES

(1) Gould, C.; Umscheid, C.; Agarwal, R.; Kuntz, G.; Pegues, D.; Brennan, P.; Bell, M.; Burns, L.; Elward, A.; Engel, J.; Lundstrom, T.; Gordon, S.; Mccarter, Y.; Murphy, D.; Olmsted, R.; Alexander, D.; Ramsey, K.; Singh, N.; Soule, B.; Schecter, W. Guideline for Prevention of Catheter-associated Urinary Tract Infections 2009. *Infect. Control Hosp. Epidemiol.* **2010**, *31*, 319−326.

(2) Foxman, B. Epidemiology of Urinary Tract Infections: Incidence, Morbidity, and Economic Costs. *DM, Dis.-Mon.* **2003**, *49*, 53−70.

(3) Zhu, Z.; Wang, Z.; Li, S.; Yuan, X. Antimicrobial Strategies for Urinary Catheters. *J. Biomed. Mater. Res., Part A* **2019**, *107*, 445−467.

(4) Singha, P.; Locklin, J.; Handa, H. A Review of the Recent Advances in Antimicrobial Coatings for Urinary Catheters. *Acta Biomater.* **2017**, *50*, 20−40.

(5) Banerjee, I.; Pangule, R. C.; Kane, R. S. Antifouling Coatings: Recent Developments in the Design of Surfaces That Prevent Fouling by Proteins, Bacteria, and Marine Organisms. *Adv. Mater.* **2011**, *23*, 690−718.

(6) Desai, D.; Liao, K.; Cevallos, M.; Trautner, B. Silver or Nitrofurazone Impregnation of Urinary Catheters Has a Minimal Effect on Uropathogen Adherence. *J. Urol.* **2010**, *184*, 2565−2571.

(7) Linsenmeyer, T. A. Catheter-associated Urinary Tract Infections in Persons with Neurogenic Bladders. *J. Spinal Cord Med.* **2018**, *41*, 132−141.

(8) Siddiq, D. M.; Darouiche, R. O. New Strategies to Prevent Catheter-associated Urinary Tract Infections. *Nat. Rev. Urol.* **2012**, *9*, 305−314.

(9) Lopez, A. I.; Kumar, A.; Planas, M. R.; Li, Y.; Nguyen, T. V.; Cai, C. Biofunctionalization of Silicone Polymers Using Poly-(amidoamine) Dendrimers and a Mannose Derivative for Prolonged Interference against Pathogen Colonization. *Biomaterials* **2011**, *32*, 4336−4346.

(10) Zhu, Z.; Wang, J.; Lopez, A.; Yu, F.; Huang, Y.; Kumar, A.; Li, S.; Zhang, L.; Cai, C. Surfaces Presenting α-Phenyl Mannoside Derivatives Enable Formation of Stable, High Coverage, Non-pathogenic *Escherichia Coli* Biofilms against Pathogen Colonization. *Biomater. Sci.* **2015**, *3*, 842−851.

(11) Zhu, Z.; Yu, F.; Chen, H.; Wang, J.; Lopez, A.; Chen, Q.; Li, S.; Long, Y.; Darouiche, R.; Hull, R.; Zhang, L.; Cai, C. Coating of Silicone with Mannoside-PAMAM Dendrimers to Enhance Formation of Non-pathogenic *Escherichia coli* Biofilms against Colonization of Uropathogens. *Acta Biomater.* **2017**, *64*, 200−210.

(12) Klemm, P.; Schembri, M. A. Bacterial Adhesins: Function and Structure. *Int. J. Med. Microbiol.* **2000**, *290*, 27−35.

(13) Choudhury, D.; Thompson, A.; Stojanoff, V.; Langermann, S.; Pinkner, J.; Hultgren, S. J.; Knight, S. D. X-ray Structure of the FimC-FimH Chaperone-Adhesin Complex from Uropathogenic *Escherichia coli*. *Science* **1999**, *285*, 1061−1066.

(14) Geibel, S.; Procko, E.; Hultgren, S. J.; Baker, D.; Waksman, G. Structural and Energetic Basis of Folded-protein Transport by the FimD Usher. *Nature* **2013**, *496*, 243−246.

(15) Wellens, A.; Garofalo, C.; Nguyen, H.; Van Gerven, N.; Slättegård, R.; Hernalsteens, J.-P.; Wyns, L.; Oscarson, S.; De Greve, H.; Hultgren, S.; Bouckaert, J. Intervening with Urinary Tract Infections Using Anti-Adhesives Based on the Crystal Structure of the FimH−Oligomannose-3 Complex. *PLoS One* **2008**, *3*, No. e2040.

(16) Fiege, B.; Rabbani, S.; Preston, R. C.; Jakob, R. P.; Zihlmann, P.; Schwardt, O.; Jiang, X.; Maier, T.; Ernst, B. The Tyrosine Gate of the Bacterial Lectin FimH: A Conformational Analysis by NMR Spectroscopy and X-ray Crystallography. *ChemBioChem* **2015**, *16*, 1235−1246.

(17) Schonemann, W.; Cramer, J.; Muhlethaler, T.; Fiege, B.; Silbermann, M.; Rabbani, S.; Datwyler, P.; Zihlmann, P.; Jakob, R. P.; Sager, C. P.; Smiesko, M.; Schwardt, O.; Maier, T.; Ernst, B. Improvement of Aglycone pi-Stacking Yields Nanomolar to Sub-nanomolar FimH Antagonists. *ChemMedChem* **2019**, *14*, 749−757.

(18) Han, Z.; Pinkner, J. S.; Ford, B.; Obermann, R.; Nolan, W.; Wildman, S. A.; Hobbs, D.; Ellenberger, T.; Cusumano, C. K.; Hultgren, S. J.; Janetka, J. W. Structure-based Drug Design and Optimization of Mannoside Bacterial FimH Antagonists. *J. Med. Chem.* **2010**, *53*, 4779−4792.

(19) Klein, T.; Abgottspon, D.; Wittwer, M.; Rabbani, S.; Herold, J.; Jiang, X.; Kleeb, S.; Lüthi, C.; Scharenberg, M.; Bezençon, J.; Gubler, E.; Pang, L.; Smiesko, M.; Cutting, B.; Schwardt, O.; Ernst, B. FimH Antagonists for the Oral Treatment of Urinary Tract Infections: from Design and Synthesis to *In vitro* and *In vivo* Evaluation. *J. Med. Chem.* **2010**, *53*, 8627−41.

(20) Han, Z.; Pinkner, J. S.; Ford, B.; Chorell, E.; Crowley, J. M.; Cusumano, C. K.; Campbell, S.; Henderson, J. P.; Hultgren, S. J.; Janetka, J. W. Lead Optimization Studies on FimH Antagonists: Discovery of Potent and Orally Bioavailable Ortho-substituted Biphenyl Mannosides. *J. Med. Chem.* **2012**, *55*, 3945−3959.

(21) Sauer, M. M.; Jakob, R.P.; Luber, T.; Canonica, F.; Navarra, G.; Ernst, B.; Unverzagt, C.; Maier, T.; Glockshuber, R. Binding of the Bacterial Adhesin FimH to Its Natural, Multivalent High-Mannose Type Glycan Targets. *J. Am. Chem. Soc.* **2019**, *141*, 936−944.

(22) Bouckaert, J.; Berglund, J.; Schembri, M.; De Genst, E.; Cools, L.; Wuhrer, M.; Hung, C. S.; Pinkner, J.; Slättegård, R.; Zavialov, A.; Choudhury, D.; Langermann, S.; Hultgren, S. J.; Wyns, L.; Klemm, P.; Oscarson, S.; Knight, S. D.; De Greve, H. Receptor Binding Studies Disclose a Novel Class of High-Affinity Inhibitors of the *Escherichia coli* FimH Adhesin. *Mol. Microbiol.* **2005**, *55*, 441−455.

(23) Touaibia, M.; Wellens, A.; Shiao, T. C.; Wang, Q.; Sirois, S.; Bouckaert, J.; Roy, R. Mannosylated G(0) Dendrimers with Nanomolar Affinities to *Escherichia coli* FimH. *ChemMedChem* **2007**, *2*, 1190−1201.

(24) Aprikian, P.; Tchesnokova, V.; Kidd, B.; Yakovenko, O.; Yarov-Yarovoy, V.; Trinchina, E.; Vogel, V.; Thomas, W.; Sokurenko, E. Interdomain Interaction in the FimH Adhesin of *Escherichia coli* Regulates the Affinity to Mannose. *J. Biol. Chem.* **2007**, *282*, 23437−23446.

(25) Jiang, X.; Abgottspon, D.; Kleeb, S.; Rabbani, S.; Scharenberg, M.; Wittwer, M.; Haug, M.; Schwardt, O.; Ernst, B. Antiadhesion Therapy for Urinary Tract Infections a Balanced PK/PD Profile Proved to Be Key for Success. *J. Med. Chem.* **2012**, *55*, 4700−4713.

(26) Kalas, V.; Pinkner, J. S.; Hannan, T. J.; Hibbing, M. E.; Dodson, K. W.; Holehouse, A. S.; Zhang, H.; Tolia, N. H.; Gross, M. L.; Pappu, R. V.; Janetka, J.; Hultgren, S. J. Evolutionary fine-tuning of conformational ensembles in FimH during host-pathogen interactions. *Sci. Adv.* **2017**, *3*, e1601944.

(27) Hospenthal, M. K.; Waksman, G. The Remarkable Biomechanical Properties of the Type 1 Chaperone-Usher Pilus: A Structural and Molecular Perspective. *Microbiol. Spectrum* **2019**, *7*, DOI: 10.1128/microbiolspec.PSIB-0010-2018

(28) Sethman, C. R.; Doyle, R. J.; Cowan, M. M. Flow Cytometric Evaluation of Adhesion of *Streptococcuspyogenes* to Epithelial Cells. *J. Microbiol. Methods* **2002**, *51*, 35−42.

(29) Beloin, C.; Houry, A.; Froment, M.; Ghigo, J.-M.; Henry, N. A Short Time Scale Colloidal System Reveals Early Bacterial Adhesion Dynamics. *PLoS Biol.* **2008**, *6*, No. e167.

(30) Xie, X.; Möller, J.; Konradi, R.; Kisielow, M.; Franco-Obregón, A.; Nyfeler, E.; Mühlebach, A.; Chabria, M.; Textor, M.; Lu, Z.; Reimhult, E. Automated Time-resolved Analysis of Bacteria−substrate Interactions Using Functionalized Microparticles and Flow Cytometry. *Biomaterials* **2011**, *32*, 4347−4357.

(31) Scharenberg, M.; Abgottspon, D.; Cicek, E.; Jiang, X.; Schwardt, O.; Rabbani, S.; Ernst, B. A Flow Cytometry-based Assay for Screening FimH Antagonists. *Assay Drug Dev. Technol.* **2011**, *9*, 455−464.

(32) Davey, H. M.; Kell, D. B. Flow Cytometry and Cell Sorting of Heterogeneous Microbial Populations: The Importance of Single-cell Analyses. *Microbiol. Rev.* **1996**, *60*, 641−696.

(33) Brown, J. M.; Hoffmann, W. D.; Alvey, C. M.; Wood, A. R.; Verbeck, G. F.; Petros, R. A. One-bead, One-compound Peptide Library Sequencing via High-pressure Ammonia Cleavage Coupled to Nanomanipulation/Nanoelectrospray Ionization Mass Spectrometry. *Anal. Biochem.* **2010**, *398*, 7−14.
(34) Kaprelyants, A. S.; Kell, D. B. The Use of 5-Cyano-2,3-ditolyl Tetrazolium Chloride and Flow Cytometry for the Visualisation of Respiratory Activity in Individual Cells of *Micrococcus luteus*. *J. Microbiol. Methods* **1993**, *17*, 115−122.
(35) Flemming, H. C.; Wingender, J.; Szewzyk, U.; Steinberg, P.; Rice, S. A.; Kjelleberg, S. Biofilms: An Emergent Form of Bacterial Life. *Nat. Rev. Microbiol.* **2016**, *14*, 563−575.
(36) Carniello, V.; Peterson, B. W.; van der Mei, H. C.; Busscher, H. J. Physico-chemistry from Initial Bacterial Adhesion to Surface-programmed Biofilm Growth. *Adv. Colloid Interface Sci.* **2018**, *261*, 1−14.
(37) Mi, H. Y.; Muruganujan, A.; Huang, X. S.; Ebert, D.; Mills, C.; Guo, X. Y.; Thomas, P. D. Protocol Update for Large-scale Genome and Gene Function Analysis with the PANTHER Classification System (v.14.0). *Nat. Protoc.* **2019**, *14*, 703−721.
(38) Chang, C. Y. Surface Sensing for Biofilm Formation in *Pseudomonas aeruginosa*. *Front. Microbiol.* **2018**, *8*, 2671.
(39) Crouzet, M.; Claverol, S.; Lomenech, A. M.; Le Senechal, C.; Costaglioli, P.; Barthe, C.; Garbay, B.; Bonneu, M.; Vilain, S. *Pseudomonas aeruginosa* Cells Attached to a Surface Display a Typical Proteome Early as 20 minutes of Incubation. *PLoS One* **2017**, *12*, No. e0180341.

https://dx.doi.org/10.1021/acsami.9b17868
ACS Appl. Mater. Interfaces 2020, 12, 21300−21310